We are IntechOpen, the world's leading publisher of Open Access books
Built by scientists, for scientists

6,900
Open access books available

185,000
International authors and editors

200M
Downloads

154
Countries delivered to

Our authors are among the

TOP 1%
most cited scientists

12.2%
Contributors from top 500 universities

BOOK CITATION INDEX
CLARIVATE ANALYTICS
INDEXED

WEB OF SCIENCE™

Selection of our books indexed in the Book Citation Index
in Web of Science™ Core Collection (BKCI)

Interested in publishing with us?
Contact book.department@intechopen.com

Numbers displayed above are based on latest data collected.
For more information visit www.intechopen.com

Single-Particle States and Elementary Excitations in Graphene Bi-Wires: Minding the Substrate

Cesar E.P. Villegas and Marcos R.S. Tavares
Universidade Federal do ABC,
Centro de Ciências Naturais e Humanas, Santo André, São Paulo
Brazil

1. Introduction

Graphene has become a subject of intense theoretical and experimental interest since it was realized in laboratory in 2004 (Novoselov et al., 2004). As being considered as a true two-dimensional (2D) material, researchers worldwide have focused their work on studying its electronic properties and the promising technological applications in designing nanoelectronic devices based on it (Castro Neto et al., 2009; Castro Neto, 2010; Peres, 2010). In fact, such studies revealed that graphene is a zero-gap 2D semiconductor. Furthermore, novel and intriguing effects concerning ballistic transport (Miao et al., 2007), the absence of Anderson localization (Beenakker, 2008), the anomalous electron-electron (e-e) interaction (Das Sarma et al., 2010), and so on, have also attracted much attention. Most of these effects arise as a consequence of the graphene band structure, in which the energy presents pretty linear dispersion relation around the Dirac point. As a direct consequence, the low-lying excitations can be described, in the first place, by the 2D Dirac-Weyl Hamiltonian, and the quasiparticles in graphene being described as massless fermions (Semenoff, 1984).

Also, it turned out to be very common to tune the carrier densities in graphene by manipulating local gate voltages (Novoselov et al., 2004; Williams et al., 2007). This led to the creation of tunable graphene-based microstructures. By the same token, it was not surprising to see that, for a perpendicular incidence of flowing quasiparticles across the electrostatic barrier, the absence of backscattering might led to a perfect transmission (Katsnelson et al., 2006) through the barrier. Indeed, the localization of electron (or hole) states by electrostatic quantum confinement in graphene turned out to be a challenging task by virtue of Klein tunneling. But, recent experimental results (Williams et al., 2011) have shown the real possibility of creating electronic waveguides by using electrostatic gates in graphene with pretty much high efficiency. The waveguide is realized by controlling the charge density in the sample through an external gate, which forms a *p-n-p* junction. In this quasi-one-dimensional (Q1D) channel, the Fermi-energy mismatching across the junction serves as a refraction index to quantify the guidance efficiency loss. Although the conductance along the wire is treated as ballistic in this case, it has been mentioned that effects such as: (i) junction roughness (Williams et al., 2011); (ii) the interaction between the graphene sheet and the underlying substrate (Chiu et al., 2010) ; and (iii) the charge-charge correlation might affect the guidance efficiency (Zhang & Fogler, 2008).

As a matter of fact, the effects induced by the electron-electron (e-e) correlation in these doped Q1D systems have been subject of intense theoretical study. (Zhang & Fogler, 2008) The most fundamental quantity to study e-e correlation is the dielectric function, which should provide us with the dynamical screening properties of the Fermionic system embedded in the sample. In fact, such a quantity has been defined, within the random phase approximation (RPA), at zero and non-zero temperature, and for doped and undoped samples with the presence of the spin-orbit interaction and strain (Das Sarma et al., 2010)(Hwang & Das sarma, 2007)(Pellegrino et al., 2010)(Brey & Fertig, 2007).

Effects induced by the interaction between graphene sheet and the underlying substrate are also an important issue which is being very addressed recently. There have been much experimental concern about substrate induced effects on the graphene sheets. Anisotropic effects have been observed (Yang et al., 2010)(Villegas et al., 2010) on the conductivity and claimed to be induced by the interaction between the graphene sheet and the underlying substrate.

This chapter focuses on the study of the electronic properties of confined electrons in bi-wires based on graphene. We theoretically propose a model to describe two coupled waveguides (quantum wires) based on graphene which has eventually been deposited over some sort of substrate. The graphene-substrate interaction is considered here through a phenomenological parameter which is taken into account in an *ad-hoc* manner. (Villegas et al., 2010) The first section is devoted to review the main points on how to confine electrons in graphene through electrostatic gate potentials. The second section presents our model and shows the single particle spectra of graphene bi-wires, taking into account the graphene-substrate interaction phenomenologically in the Dirac hamiltonian, whose solution is given by a pseudo-spinor. Such an effect can be induced in the sample by considering the interaction between the graphene sheet and the substrate such as boron nitrate (BN) (Giovannetti et al., 2007). Furthermore, in order to control the pseudo-spinor components in the barrier region, we theoretically explore and manage the interaction between the substrate and the graphene sheet, considering it in order to keep a reasonable guiding efficiency. We then study, in Sec. III, the dynamical screening properties of the Fermion gas which is eventually laid in the structure. We calculate the dielectric response function within the RPA, which turned out to be a good approximation describing e-e correlations in graphene even for small charge densities (Hwang & Das sarma, 2007). The roots of this function provide us with the collective excitations in the system. Our results show that the graphene-substrate interaction induced effects play an important role in obtaining the bare Coulomb potential and the dielectric function of the system. Such a role manifests itself in the dispersion relation of the optical and acoustical plasmon modes. We found that the graphene-substrate interaction might eventually increase the damping effects on these modes.

2. Electrostatic confinement of electrons in graphene

Nano-engineering serves to yield structures that are not found *in natura* anywhere. Indeed, most of such structures have been realized as an essential feature of quantum mechanics, i.e., they are a result of quantum confinement, which constitutes the basic building block of electronic devices. Although in graphene the quantum confinement by electrostatic potentials seems to be a difficult job by virtue of the absence of backscattering, which is a direct consequence of pseudo-chiral behavior of quasiparticles, many theoretical (Pereira et al.,

2007) and experimental (Williams et al., 2011) works have attempted proposed different approaches to study and overcome this difficulty. In the following, we discuss the main points regarding these proposals.

2.1 Etched structures

Etching the graphene leads to the formation of 1D quantum wires. These structures are commonly mentioned in the literature as graphene nanoribbons (GNRs) (Brey & Fertig, 2006). It is well known that the semiconducting gap in GNRs is strongly dependent on the ribbon width, and also on the kind of the ribbon edge (Son & Cohen, 2006). The ribbon depends on the kind of the edge termination, leading to different boundary conditions. Since the graphene is a hexagonal bound of carbon atoms, two types of termination can be etched: the armchair and the zig-zag terminations. It has been shown that the narrower the ribbon, the bigger the semiconducting gap. Moreover, very narrow GNRs evidenced the existence of surface states and miniband formation in the long wavelength limit $\mathbf{k} \rightarrow \mathbf{0}$. (Brey & Fertig, 2006) As a matter of fact, the combination between ribbon width and edge termination turned out to be a crucial point in determining if the sample is metallic or semiconductor. Therefore, etching these structures requires very sensible controlling of the edge termination, and do not assure a standard technique in obtaining identical materials. This may be now-days the main disadvantage in etching graphene structure to produce 1D quantum structures producing the same kind of material.

2.2 Infinite mass boundary conditions

The infinite mass boundary condition approach was proposed by Berry and Mondragon (Berry & Mondragon, 1987) in order to overcome the difficulty in confining neutrino relativistic billiards. They considered the possibility of taking into account the neutrino quasi-mass induced effects in theoretically treating the electrostatic gate potential $V(x)$. The neutrino mass term $M(x)$ was considered to be x-coordinate dependent, so that the effective gate potential might be written as $V^{eff}(x) \rightarrow V(x) + M(x)c^2\sigma_z$, where c is the light velocity and σ_z the z-direction Pauli matrix. The same approach can be used to study the gate potential providing charge confinement in graphene (Peres et al., 2009). In principle, such a gate potential should form a long stripe based on graphene. We schematically show $V^{eff}(x)$ in Fig.1 and simply picture the different regions regarding the mass term $M(x)$. To graphene, one assumes the light velocity $c \rightarrow v_F = 1.1x10^6 m/s$. In region II the mass term $M(x)$ can be considered zero by virtue of vanishing graphene-substrate interaction, while in regions I and III it can assume finite values. Notice that in the case of neutrinos, the $M(x)$ was considered to be infinite (hard wall approach), since they theoretically sought for vanishing the Fermi velocity outside the well. In this sense, it was claimed that this kind of technique might lead to the confinement of charges to region II, because the effective potential should be strong enough to enable wavefunction reflection at the interface of the potential (at $x = \pm L/2$). The difference between this technique and the one presented above concerns to the ribbon (or stripe) edge. Here, the edge termination does not play the same role as in the previous case, and the boundary conditions are the same as in the standard quantum well (or finite mass) confinement (Lin et al., 2008). We finally recall that the gate potential naturally imposes the continuity of the wavefunction at the interfaces $x = \pm L/2$, but not of its derivative.
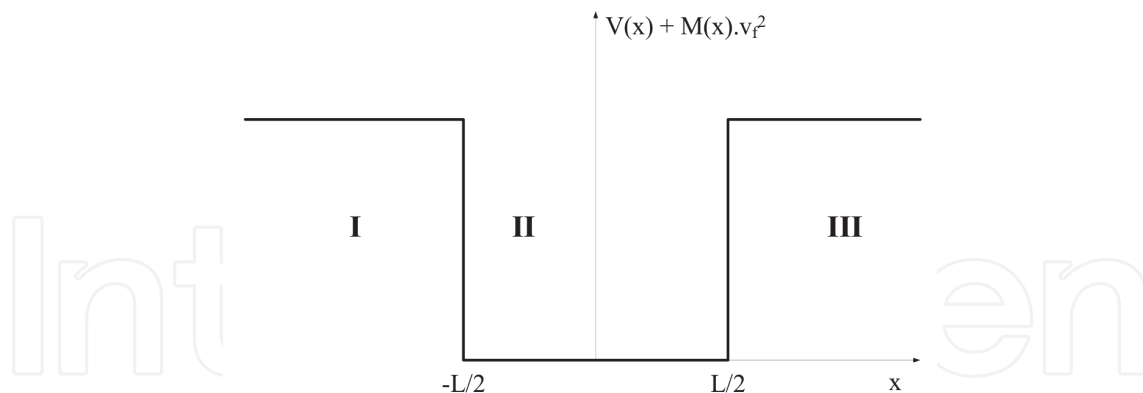
$$V(x) + M(x).v_f^2$$

```
         ┌─────────┐              ┌──────────────┐
    I    │    II   │              │     III      │
         │         │              │              │
         └─────────┘              └──────────────┘
       -L/2                     L/2            x
```

Fig. 1. Schematic representation of the infinite mass confinement potential profile. The mass *M* is zero in region II and infinite elsewhere.

2.3 Graphene-substrate interaction

Another usual technique improving confinement of electrons in graphene is to help opening up a semiconducting gap in the energy spectrum. In particular, it was shown that the most effective way to do that is to have the graphene, and its eventual substrate, embedded in boron nitrate material (Giovannetti et al., 2007), provided it is also a hexagonal lattice. The interaction between the different atoms in the whole sample causes then an anisotropy associated to the different number of electrons in the sublattices *A* and *B* that form the unit cell of the graphene honeycomb (Semenoff, 1984). That is responsible to open up the gap. Experiments have shown that this induced gap can vary from 50 up to 260 meV (Lu et al., 2007; Zhou et al., 2007). We mention that the effects of such asymmetry in the sublattices can be theoretically incorporated into the Dirac Hamiltonian by considering a sort of phenomenological (or *quasi-mass*) parameter $\Delta\sigma_z$ in an ad-hoc manner. It is worth to mention that this parameter $\Delta\sigma_z$ has the same nature as those representing the Rashba spin-orbit interaction in graphene (Kane & Mele, 2005; Min et al., 2006).

2.4 Tuning the Fermi level in p-n junctions

A recent theoretical proposal to improve and study the confinement of electrons in graphene is based on the so-called Goos-Hanchen (GH) effect (Goos & Hanchen, 1947). The GH effect has been shown for the first time back in the 40s and accounts for a universal shift that a light beam, which is reflected from a given medium, can suffer. Such a shift can be attributed to a sort of residual transmission into the medium which has the lower refractive index, causing the evanescence of the electromagnetic wave. The electronic analogy of the GH effect can also manifest itself in graphene *p-n-p* junctions (Beenakker et al., 2006). As it was mentioned, electrostatic gates actually control the charge-type doping in the graphene and eventually create a *p-n* junction. In such structures, the Fermi energy plays the role of a refraction index, since it assumes different values as it crosses the junction. The main advantage of this technique is that it enables one to easily control the carrier density in the sample, providing the designing of *electronic* waveguide structures. As a mater of fact, recent experiments have shown the possibility of creating waveguides in graphene *p-n-p* junctions, leading to a variety of promising applications (Cheianov et al., 2007; Williams et al.,

2011). Such a work also dealt with the direction-dependent transmission induced effects in graphene (Pereira et al., 2007). In any case, it was shown that, by tuning the Fermi energy in given *p-n-p* junctions, it was certainly possible to form electronic waveguides with reasonable efficiency in graphene, leading to the promising fabrication of nanodevices based on electronic confinement in graphene.

3. Single particle spectra in graphene quantum wires

In response to the points discussed above and motivated by the promising applications of quantum confinement in graphene, we study below the single particle spectrum of quasi-confined electrons in graphene *p-n-p* junctions. We consider an electrostatic gate potential, whose some sort of arrangement can eventually be responsible for forming two quantum wires (double *p-n-p* junctions) coupled by a barrier of width L_b and height V_b. Our model also deals with a more generic situation where the interaction between the substrate and graphene sheet is properly considered in both doped regions .
The low-energy band structure for a single valley[1] (*K* point) in graphene can be described by the 2D Dirac-like Hamiltonian (Semenoff, 1984) in the form

$$H_{2D} = \gamma \begin{pmatrix} 0 & k_x - ik_y \\ k_x + ik_y & 0 \end{pmatrix} + \beta\sigma_z, \tag{1}$$

where σ_z is the Pauli matrix, $\gamma = \sqrt{3}\hbar a_0 t/2$ is a parameter associated to the lattice constant $a_0 = 0.246$ nm and to the nearest neighbor hopping energy $t \approx 2.8$ eV in graphene. As mentioned before, the parameter β accounts for an asymmetry associated to different number of electrons in sublattices *A* and *B*, that form the unit cell of the honeycomb. The values for β might be strongly dependent on the substrate over which the graphene sheet is embedded. The stronger is the interaction between graphene sheet and the substrate, the larger is the β parameter which is responsible for opening an energy gap in the Dirac cone spectrum. This is the parameter which will quantify here, in an *ad-hoc* manner, the graphene-substrate interaction strength. In this way, one should be able to investigate such effects theoretically by considering the parameter $\beta \neq 0$ in the Eq. (1). Therefore, the effects associated to the mentioned parameter will be carefully studied here.

3.1 Triple barrier (Double well)

In order to study the electronic guidance in double coupled waveguides based on graphene, one should be able to seek the effects of imposing a confinement potential $U(x)$, as pictured in Fig.(2), onto the Hamiltonian H_{2D}. This potential $U(x)$, as generated by electrostatic gates, leads to two transversal quantum wires along the *y*-direction with widths L_1 and L_2 separated by a barrier of length L_b. The tunable barrier between the wires, the region *III* on Fig.(2), is assumed to be responsible for controlling the coupling between the two *p-n* junctions. As mentioned above, the issue of weather the epitaxially-growth graphene can or cannot be gated is not important here, because one can ad-hocly assigned the parameter β to other phenomenological effects as well, such as the spin-orbit interaction, the impurities or imperfections in the sample, and so forth (Ziegler, 1996). Therefore, the eigenstates of

---

[1] It should be pointed out that the two lattice points K and K′ decouple from each other in the graphene Hamiltonian (1) only when the disorder generated by the potential is much smaller than the lattice parameter (Ando & Nakanishi, 1998).
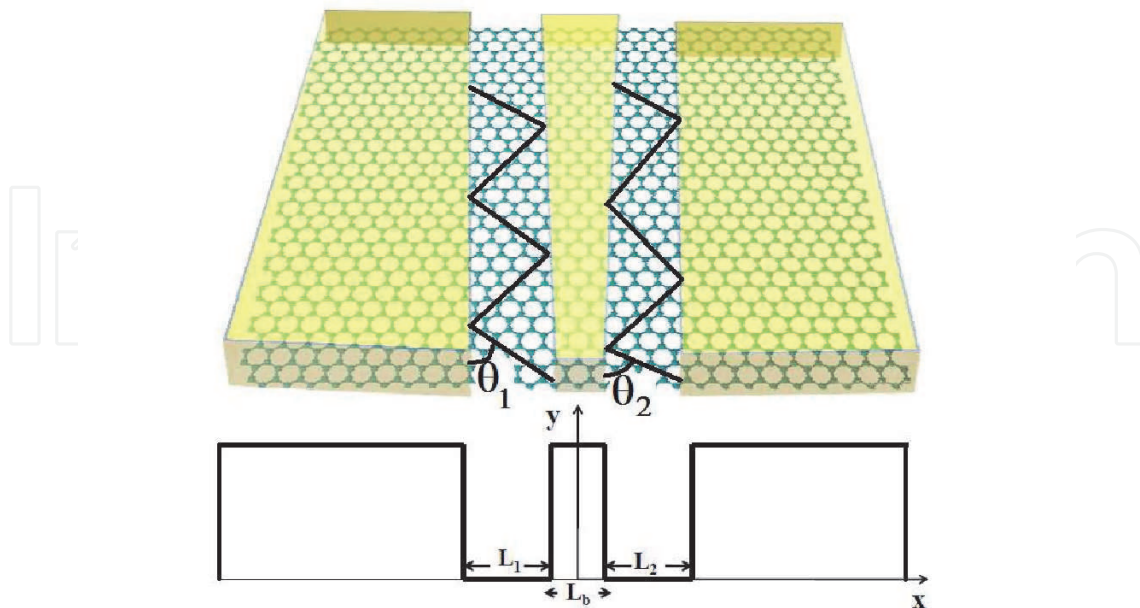
Fig. 2. Schematic representation of the potential profile forming a biwaveguide based on graphene. It shows two coupled channels of widths L_1 and L_2, separated by a barrier of width L_b and height U_0. Two different reflection angles θ_1 and θ_2 can be considered in the regions II and IV, respectively, by virtue of different graphene-substrate interaction strength.

the Hamiltonian $H = H_{2D} + U(x)$ can be written as a two-component spinor in the form (Villegas & Tavares, 2010; Villegas et al., 2010)

$$|\psi(x,y)> \; \simeq e^{ik_y y} \begin{bmatrix} \chi_A(x) \\ \chi_B(x) \end{bmatrix}, \tag{2}$$

where $\chi_A(x)$ and $\chi_B(x)$ are the pseudo-spin wavefunction components. Here we choose expressions for $\chi_A(x)$ and $\chi_B(x)$ that naturally satisfies the secular equation $H|\psi(x,y) > = E|\psi(x,y) >$ and represent electronic states that are confined by the potential $U(x)$. It should be recalled at this point that the Fermi level in the sample should play the role of a refraction index and, as consequence, the quasiparticles might undergo to internal reflections as they eventually cross the potential interfaces, giving rise to the phenomena analogous to the GH shift discussed above. Thus, the wavefunctions for the component $\chi_A(x)$ in different regions, can be written in terms of stationary functions within the well regions and evanescent functions within the barrier region, i.e.,

$$\chi_A(x) \sim \begin{cases} C_I e^{\kappa_I x} & region \;\; I \\ C_{II} \sin q_{II} x + D_{II} \cos q_{II} x & region \;\; II \\ C_{III} e^{\kappa_{III} x} + D_{III} e^{-\kappa_{III} x} & region \;\; III \\ C_{IV} \sin q_{IV} x + D_{IV} \cos q_{IV} x & region \;\; IV \\ D_V \, e^{-\kappa_V x} & region \;\; V \end{cases} \tag{3}$$
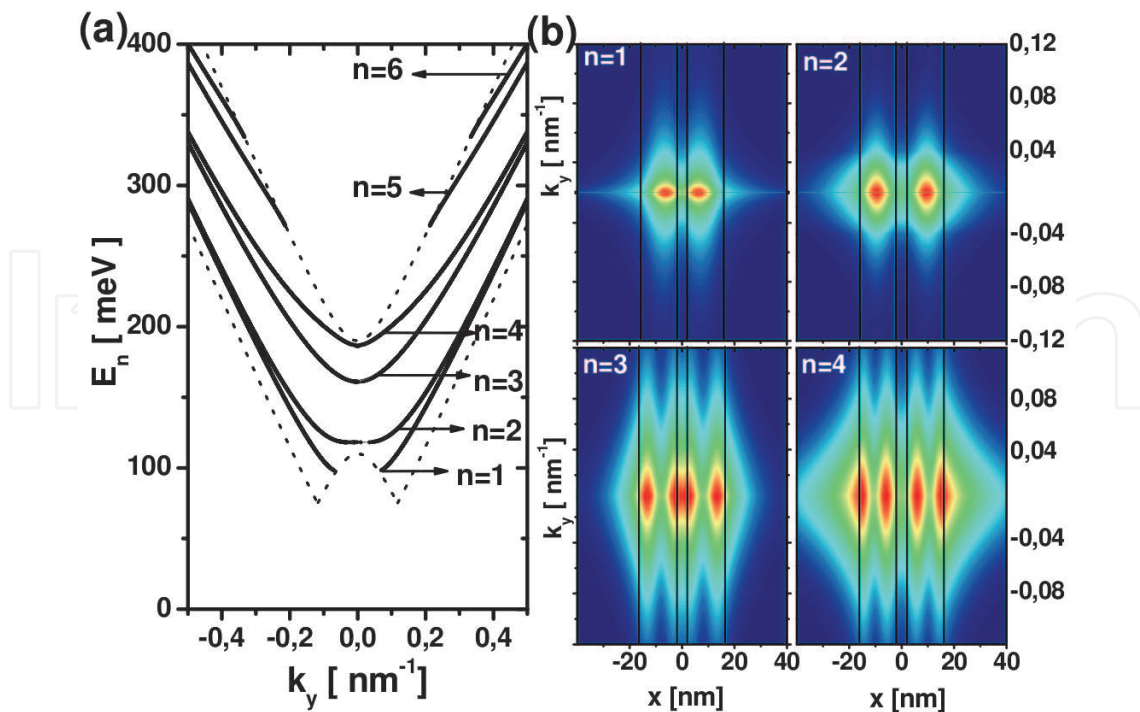
Fig. 3. (Color online) (a) Dispersion relations, $E_n(k_y)$, for a symmetric structure with $L_1 = L_2 = 14$ nm, $L_b = 4$ nm, and $U_0 = 150$ meV. Here, $\beta = 40$ meV over all layers in the structure. The dashed lines represent the edges of the regions where the confined state branches lay down. (b) Probability density function $\rho_{nk_y}(x)$ for $n = 1, ..., 4$, plotted in arbitrary units, showing the spreading of states in the graphene wires. Thin vertical lines indicate the position of the potential edges.

Here, the wavevector along the x-direction

$$\kappa_i = \gamma^{-1}\sqrt{(\gamma k_y)^2 + (\beta_i)^2 - \left[E(k_y) - U_0\right]^2} \tag{4}$$

for $i = I, III, V$ and

$$q_j = \gamma^{-1}\sqrt{E(k_y)^2 - (\gamma k_y)^2 - \left(\beta_j\right)^2} \tag{5}$$

for $j = II, IV$. Notice that the parameter β may assume a different value in each region and this is a form to simulate different substrate interaction strengths or dopings. Due to the perfect similarity between spin-orbit and Dirac Hamiltonians, such a parameter can be linked, in an *ad-hoc* manner, to a spin-orbit interaction occurring in the samples without gate. Finally, the set of coefficients $\{C_I, C_{II}, C_{III}, C_{IV}\}$ and $\{D_{II}, D_{III}, D_{IV}, D_V\}$ indicate the intensity of propagating and anti-propagating waves, respectively within each doped region. This type of solution for $\chi_A(x)$ in the Eq. (3) was considered before (Pereira et al., 2007) where the component χ_B is also written straightforwardly, since $H|\psi> = E|\psi>$ leads to two coupled differential equations for the components $\chi_A(x)$ and $\chi_B(x)$ which are solved through the same *anzatz* (3). The energy dispersions $E_n(k_y)$ in Eqs. (4) and (5), are obtained by imposing continuity conditions for both spinor components $\chi_A(x)$ and $\chi_B(x)$ at the edges of the confining potential $U(x)$. From these continuity conditions, one is able to write down a set of equations in the matrix form

$$\hat{M}C^T = 0, \tag{6}$$

where $\hat{M}(E_n, k_y)$ is the 8×8 matrix shown in the Appendix A and C is a 1×8 matrix formed by the amplitude of propagating and anti-propagating waves in the sequence: $(C_I, C_{II}, D_{II}, C_{III}, D_{III}, C_{IV}, D_{IV}, D_V)$. Notice that the dispersions $E_n(k_y)$ are obtained through the non-trivial solutions of the Eq. (6) and implying that

$$\det\left[\hat{M}(E_n, k_y)\right] = 0. \tag{7}$$

We use optimized numerical routines to find the n roots of Eq. (7) for a given value of the wavevector k_y.

At this point, we should define

$$\theta_n^j = \arctan(k_y / q_n^j) \tag{8}$$

as the reflection angles for the regions $j = $ II and IV. These angles are schematically indicated in Fig.(2) and represent the n possible angles of reflection in the regions $j = $ II and IV through which the guidance occurs. One can really read out from Eq. (5) that, in considering $\beta_{II} \neq \beta_{IV}$, a spatial-anisotropy induced effect should take place, as the effective depths of each potential well in the regions $j = $ II and IV are different from each other.

3.1.1 Extended states

Let us first assume an unique value for the ad-hoc parameter $\beta_{i=j} \equiv \beta = 40$ meV, for all layers shown in Fig.(2). Then we solve Eq. (7) for a given value of k_y and determine a number n of different roots. Figure 3(a) shows the first six solutions as a function of k_y and these energy dispersions, $E_n(k_y)$, map out the confined modes in the graphene double wire system described by the lateral confining potential, $U(x)$. Due to interwire tunneling, the pairs of *bound* (symmetric) and *antibound* (antisymmetric) states with energy eigenvalues E_1 and E_2, E_3 and E_4, etc, show larger (smaller) energy separation for smaller (larger) values of wavevector k_y. These energy branches were found in a region limited by the dotted lines, which are roughly given by the expressions

$$[(\gamma k_y)^2 + \beta^2]^{1/2} \tag{9}$$

and

$$\pm [(\gamma k_y)^2 + \beta^2]^{1/2} + U_0. \tag{10}$$

We stress that the inverse of the lifetime of any subband displayed in Fig. 3(a) is assumed as being of the order of the numerical precision required to solve the Eq. (7) (Nguyen et al., 2009). Although this may seem an approximation to the numerical solution, the high precision required in our calculation produces very reliable results.

The effects associated to wide states can be better addressed when the probability density function given by

$$\rho_{nk_y}(x) = |\chi_A(x)|^2 + |\chi_B(x)|^2, \tag{11}$$

is drawn for each subband n as a function of the wavevector k_y. Figure 3(b) shows $\rho_{nk_y}(x)$, plotted in arbitrary units, for the same lowest four states of Fig. 3(a), showing regions of maximum and minimum intensities for localized and quasi-extended states in our potential model. Clearly, the larger (smaller) is the wavefunction amplitude in regions I and V, the weaker (stronger) is the evidence for localization effects on the structure. The states $n = $ 1, 2, and 3 show stronger confinement to the well regions while state $n = $ 4 display the quasi-extended character with a large probability amplitude over the whole structure and a
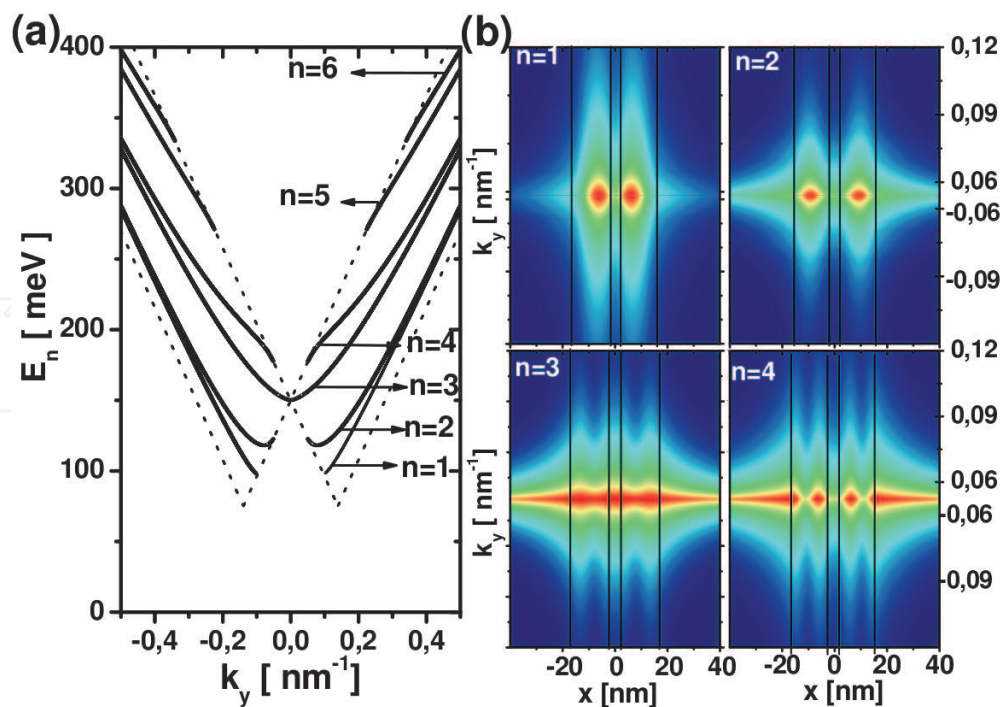
Fig. 4. (Color online) - The same energy dispersions and probability densities as in Fig. 2, but without the **substrate-graphene coupling** term ($\beta = 0$ in all layers) in the pseudo-relativistic Hamiltonian.

long-range exponential decay for small values of k_y in the regions I and V. As the wavevector $|k_y|$ increases, these extended states become more and more localized inside the well regions. In Fig. 4 we are showing the same results as in Fig. 3, but with the parameter β being zero in all regions. As noticed, the state $n = 1$ shows only a slightly larger spreading along the wires for increasing values of k_y and the state $n = 2$ increases the spreading along the wires and into the lateral barrier regions. However, the amplitude probability for states 3 and 4 show very large extended character in all regions for small values of k_y. In other words, the addition of a substrate-graphene coupling term to the Dirac-like Hamiltonian increases the lateral localization character of the extended states.

3.1.2 Anisotropic values of β : effects on the conductance

With the choice of different values for the parameter β in each region, the system should reveal interesting effects. In order to analyze these effects, we define auxiliary quantities such as $\Delta = \beta_I - \beta_{III}$, $\beta_{II} = \beta_{IV} = 0$, $\beta_I = \beta_V$ and $\beta_{III} = 10$ meV. When $\Delta \neq 0$, the interaction between graphene sheet and substrate in regions I and III have different strength values. Furthermore, one can also read out from Eq. (4) that the wavevector $\kappa_I \neq \kappa_{III}$ when $\Delta \neq 0$. This situation mimics a spatial anisotropy as if the effective barrier heights in regions I and III were different from each other. We predict that these spatial anisotropy induced by finite Δ can be verified experimentally through a measure of the electrical conductance along the y-direction. Very recently, this conductance, as a function of well width, has been investigated theoretically in one dimensional channel formed by a single graphene p-n junction without the interaction parameter β (Beenakker et al., 2006). It was shown that a minimum in the energy dispersion $E_n(k_y)$ would generate a plateau in the conductance along the channel. In addition, each minimum in the ground-state energy $E_1(k_y)$ would contribute independently with an
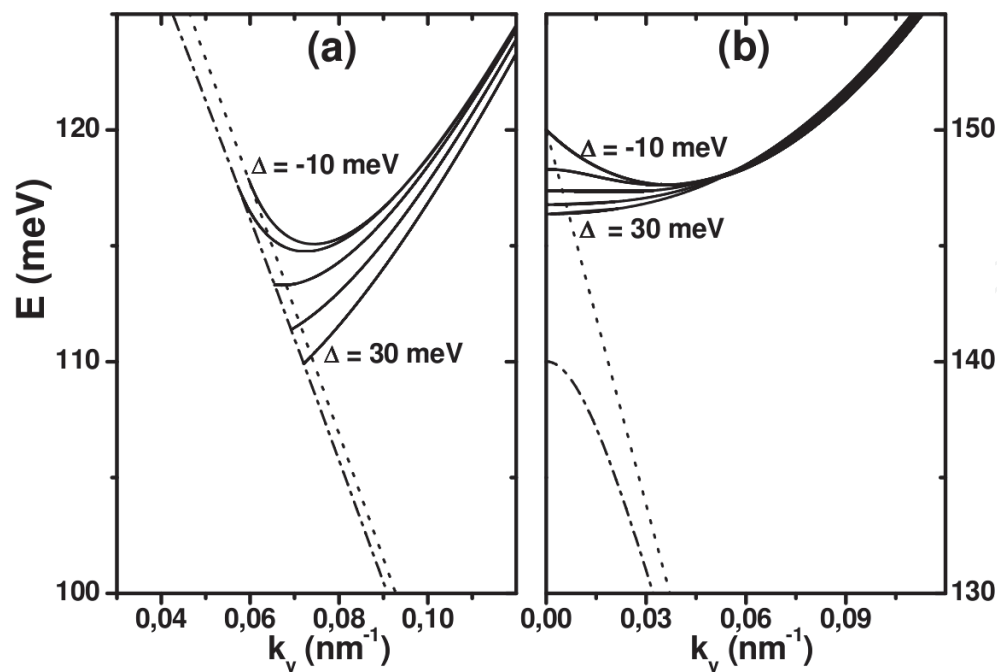
Fig. 5. (Color online) - Effects of **substrate-graphene** coupling strength on the shape of the energy dispersion in a double wire system based on graphene sheet grown over a substrate. Here, the double wire structure is symmetric with widths: $L_1 = L_2 = 9$ nm, $L_b = 4$ nm and $U_0 = 150$ meV. The **strength values**, β_i, are taken different in the layers according to: $\Delta = \beta_I - \beta_{III}$, $\beta_{II} = \beta_{IV} = 0$, $\beta_I = \beta_V$ and $\beta_{III} = 10$ meV.

amount of e^2/h per spin and per valley degrees of freedom to the conductance. Therefore, two minima in our dispersion relation $E_1(k_y)$ should be responsible for a first step in the quantum conductance at $8e^2/h$. It is claimed by (Beenakker et al., 2006) that this result can identify a novel pseudo-spin dependent scattering mechanism in graphene thus, it should manifest itself as a $8e^2/h$ conductance step in a bipolar *p-n* junction. We are sure that in coupled double wire graphene systems this conductance contribution would be simply enhanced by a factor two with a plateau occurring near $16e^2/h$ if the coupling between the wires is weak, which is not the case here.

Nevertheless, these conclusions have motivated us to study the role of the spatial anisotropy inducing modifications to the minimum found in the graphene double wire dispersion relations. We have chosen to calculate the eigenvalues $E_n(k_y)$ for narrower well layer systems where the quantum mechanical regime becomes fully achieved. In Fig. 5 we are showing only one side of the energy dispersion $E_n(k_y)$ for states $n = 1$ (panel (a)) and $n = 2$ (panel (b)) in a symmetric structure where $L_1 = L_2 = 9$ nm, $L_b = 4$ nm and $U_0 = 150$ meV. At this point we should recall that our theory can also be applied to graphene nanoribbons, whose widths are typically of the order of 5 nm (Ritter & Lyding, 2009). As the parameter Δ increases, from -10 to 30 meV in steps of 10 meV, we note minima in both energy branches being systematically destroyed. Therefore, it is possible to claim that the physical mechanisms leading to a plateau in the conductance near $16e^2/h$ will be destroyed for a finite value of Δ. Furthermore, the dotted and dash-dotted lines limit the confined states region at given critical k_y value associated to an asymmetry induced by Δ. Both dotted lines are given by Eq. (10) with the minus sign. These results evidence that, for a more general situation regarding the
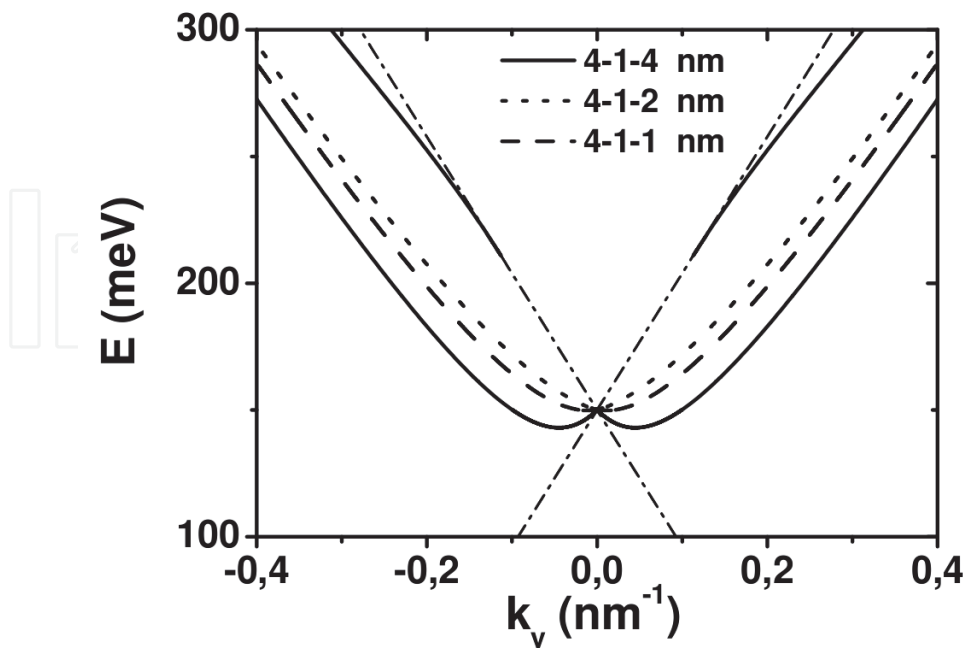
Fig. 6. (Color online) - Effects of increasing spatial anisotropy on the $E_1(k_y)$ minima for $\beta = 0$. Different indicate different values for the set of parameters $L_1 - L_b - L_2$ nm, and where $U_0 = 150$ meV.

graphene sheet and substrate interaction strength, the parameter β in the Eqs. (9) and (10) turns out to be equal to $\max(\beta_{II}, \beta_{IV})$ and $\min(\beta_I, \beta_{III})$, respectively. This informs us that the dotted energy lines limiting the confined state region can be determined by an appropriated choice of the parameter strength β. As a final test to this graphene coupled double wire model, we are showing in Fig. 6 the effects of increasing the spatial asymmetry on the ground-state double minima occurring for the structure $L_1 = 4$ nm, $L_b = 1$ nm, $L_2 = 4$ nm (referred as $4 - 1 - 4$) when we neglect any interaction between graphene sheet and the substrate in all layers of Fig. 2. As can be noted, when L_2 decreases (dashed lines), the two degenerate minima near $k_y = \pm 0.30 nm^{-1}$ merge into a single one minimum at $k_y = 0$. Therefore, in this lowest channel mode the total amount added to the conductance plateau of $16e^2/h$ for a symmetric structure $4 - 1 - 4$ will change back to the total amount $8e^2/h$ in the asymmetric structures shown in this figure.

3.1.3 Guidance efficiency

We show in Fig. 7(a) the dispersion relation E_n of the confined (guided) states (modes) in a symmetrical structure. An spatial anisotropy has been induced here by assuming $\beta_{II} = 0$ and $\beta_{IV} = 40$ meV. The branches E_n indicate the n different roots of the Eq. (7) for any given wavevector k_y. These branches were found numerically in a region limited by the long- and short-dashed lines, which are roughly given by the expressions $E = \gamma k_y$ and $E = \pm \gamma k_y + U_0$, respectively. Outside this region, the quasiparticle can be assumed to be free from the effects of $U(x)$. The intersections of these dashed lines with each branch n indicate the points (k_y, E_n) which determine, through the Eq. (8), the critical angles $\theta_c(E_n)$. The guidance through the y-direction in the whole structure is only allowed for those angles greater than $\theta_c(E_n)$. The two lowest energy branches, E_0 and E_1, get coupled strongly as the wavevector k_y increases.
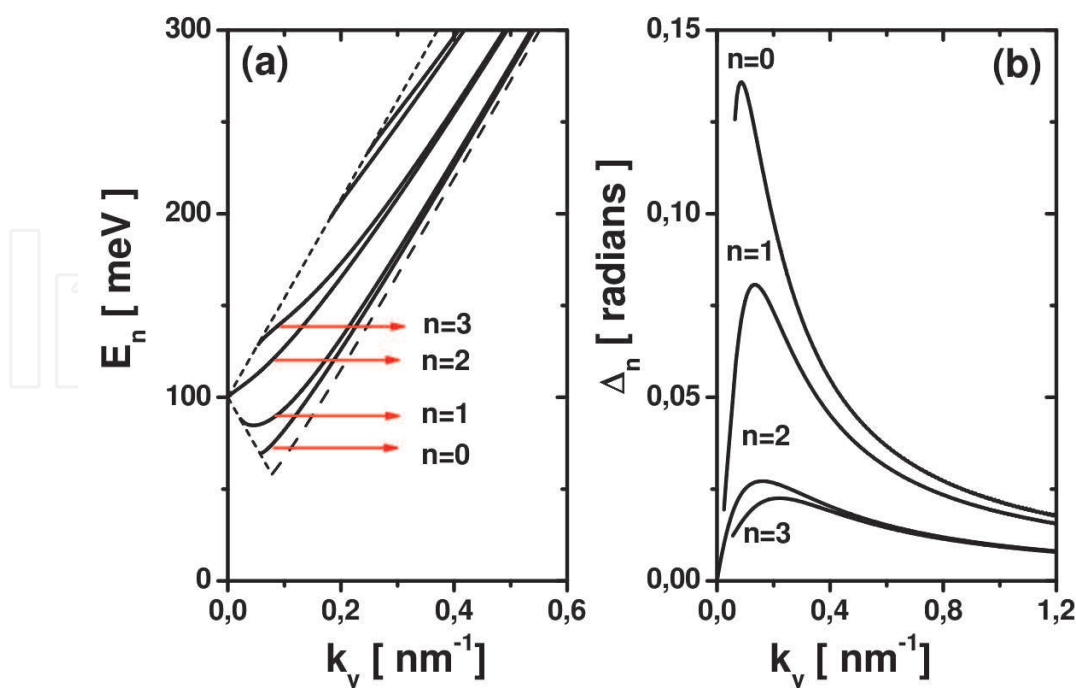
Fig. 7. (Color online) (a) The energy dispersion relation $E_n(k_y)$ for an structure whose parameters are $L_1 = L_2 = 20$ nm, $L_b = 10$ nm and $U_0 = 100$ meV. The six lowest subbands (or modes) are shown. (b) The parameter Δ_n as a function of the wavevector k_y for the 4 lowest energy modes.

The same effect occurs with the two subsequent branches E_2 and E_3. Such sort of effect is not present in the single waveguide case. Notice that, with such a spectrum, we thoroughly map out the allowed coupled guided modes in our biwire system. Furthermore, it is interesting to notice that the guided mode of the second order, $n = 2$, is the only one which is present in the long wavelength limit $k_y \to 0$, with the energy $E_{n=2}(k_y \to 0) \simeq U_0$.

It is worth to mention that, for a given value of the wavevector k_y, the reflection angles θ_n^{II} and θ_n^{IV} assume different values when $\beta_{II} \neq \beta_{IV}$. Indeed, the spatial anisotropy effect induced by considering different graphene-substrate interaction strength in each waveguide moved us to define and analyze the quantity

$$\Delta_n = \left| \theta_n^{j=II} - \theta_n^{j=IV} \right| \tag{12}$$

as a function of the wavevector k_y. It serves as an auxiliary quantity showing how the reflections in the two waveguides are actually taking place. When Δ_n is identically equal to zero, the reflections in the two waveguides are occurring strictly in phase. We plot Δ_n in Fig. 7(b) for $n = 0, 1, 2$ and 3. All parameters are the same as in Fig. 7(a). We found maxima in the Δ_n as a function of k_y for all the considered subbands n. The corresponding wavevector values of these maxima indicate the parallel momenta (or energy) for which the out-of-phase reflections in the two wires lead to the most destructive effect.

We stress that all guided modes found in Fig. 7(a), i.e., the different n branches, can be considered as of infinite lifetime since we are considering purely real energies only (Nguyen et al., 2009).

3.2 Double barrier (One well)

For the sake of completeness, we now show results for an single waveguide, of width 50 mn, in the absence of any substrate interaction, i.e., $\beta_j \equiv \beta = 0$ for all regions. To produce a single waveguide, we take the barrier width $L_b \to 0$ and the well width $L_1 = L_2 = 25$ nm. It is not difficult to realize that such parameters simply lead to the wavevector $k_y \to \gamma^{-1}E_n \sin\theta$, where θ is the reflection angle within the single waveguide defined in the Eq. (8). Therefore, we solve Eq. (7) in order to find the n different roots E_n for a given angle θ. In this way, we plot in Fig. 8(a) the dispersion relation E_n of the confined (guided) states (modes) in this single waveguide as a function of the reflection angle θ. As one can notice, there is much evidence of the existence of guided modes up to the seventh order. These modes were found in a region limited by dotted lines, which are given by $\gamma k_y + U_0$ and $U_0 - \gamma k_y$. The electrons whose energies are located outside this region are not allowed to be guided with any value for θ whatsoever. Intersections of the branches E_n with the dotted lines indicate the critical angle for each mode n. They are marked with circles in Fig. 8(a). Beyond these angles, the guidance should take place in the structure. We finally plot in Fig.8(b) the probability density function $\rho_{n\theta}(x)$ in terms of θ (instead of k_y) for the four lowest guided modes. By showing them, we completely mapped out the values of the reflection angle θ for which the guidance takes place with the most probability.
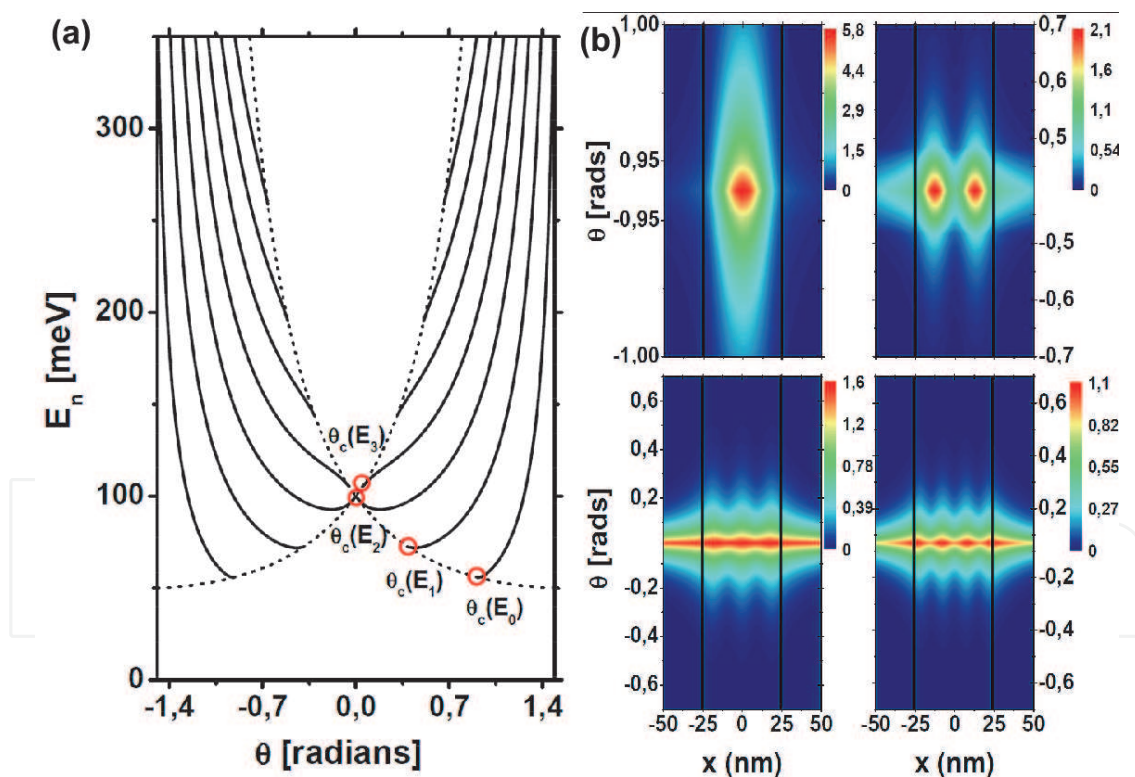

Fig. 8. (Color online) (a) The energy dispersion E_n as a function of the reflection angle θ for a single waveguide of width 50 nm. Here, $U_0 = 100$ meV. The red circles indicate the critical angles: $\theta_c(E_0) = 0.92$ rad, $\theta_c(E_1) = 0.40$ rad, $\theta_c(E_2) = 0.0$ rad and $\theta_c(E_3) = 0.05$ rad. (b) The probability density function $\rho_{n\theta}(x)$ corresponding to the 4 lowest energy branches showed in part (a).

4. Collective excitations in graphene quantum wires

Collective excitations (plasmon modes) are the most elementary excitations due to Coulomb interaction. These modes should be seen experimentally through the Raman inelastic scattering spectra (Bostwick et al., 2007). Within the linear response theory, plasmon modes can be theoretically modeled by finding out the poles of the dielectric function, which will be written here within the RPA. Since we are dealing with two coupled graphene stripes, it shall be worthy to develop below the fundamental expressions of interest in order to properly get the dielectric function (Ehrenreich & Cohen, 1959).

4.1 Triple barrier in weak tunneling regime

For the sake of simplicity, we set the solutions for the pseudo-spinor $\phi_{nk}(x)$ by assuming an extremely weak tunneling regime between the wires. In such a regime, the system can be considered as two independent waveguides. This procedure simplifies the model and represents a very feasible experimental situation in which the gate voltage, as shown in Fig.2, is increased to values up to 1 eV. The results shown in (Williams et al., 2011) supports such an approach. The graphene based waveguides turn out to be of a high efficiency, which suggests that the Klein tunneling through the barriers turn out be a less important effect. Indeed, armchair edged GNRs are considered to be no longer a gapless semiconductor. In such a regime, the pseudo-spinor components are considered to be identically zero outside both wires, including the barrier region.

Thus, we neglect the coupling between higher subbands and assume charges (electrons) occupying the lowest subband only, so that subband index n is treated here as waveguide index. The proposed analytical solutions for the pseudo-spinor can assume the following form (Villegas & Tavares, 2011):

$$\phi_{nk}(x) = \begin{pmatrix} A_n \sin k_n^0 \left[x + (-1)^{n+1} L_b/2 \right] \\ B_n k_n^0 \cos k_n^0 \left[x + (-1)^{n+1} L_b/2 \right] - k \sin k_n^0 \left[x + (-1)^{n+1} L_b/2 \right] \end{pmatrix}. \tag{13}$$

Here, the coefficients $A_n = \sqrt{2/L_n}$ and $B_n = -i\gamma A_n / [E_n + \beta]$, with $E_{n=1,2}(k) = \gamma \sqrt{k^2 + (k_n^0)^2 + (\beta \gamma^{-1})^2}$ being the hyperbolic eigenvalues of H. Notice that $k_n^0 = \pi/L_n$ is the quantized wave-vector corresponding to the fundamental quantum state in both waveguides

4.2 Linear response approach

We then start writing out the usual screened Coulomb potential for the Fermions embedded in our structure Jackson (1998),

$$V^s(r) = \frac{1}{4\pi\epsilon_0} \int dr\prime \frac{\rho(r\prime)}{|r - r\prime|}, \tag{14}$$

where ϵ_0 is the static background dielectric constant which depends on the substrate over which the graphene sheet lies (Ando, 2006). Here, the RPA density-density correlation function

$$\rho(r,\omega) = \frac{e^2}{L_y} \sum_{m,n,k,q} \psi_{mk}^*(x,y)\, \psi_{n,k+q}(x,y) \Pi_{mn}(k,q,\omega)\, V_{mn}(k,q) \tag{15}$$
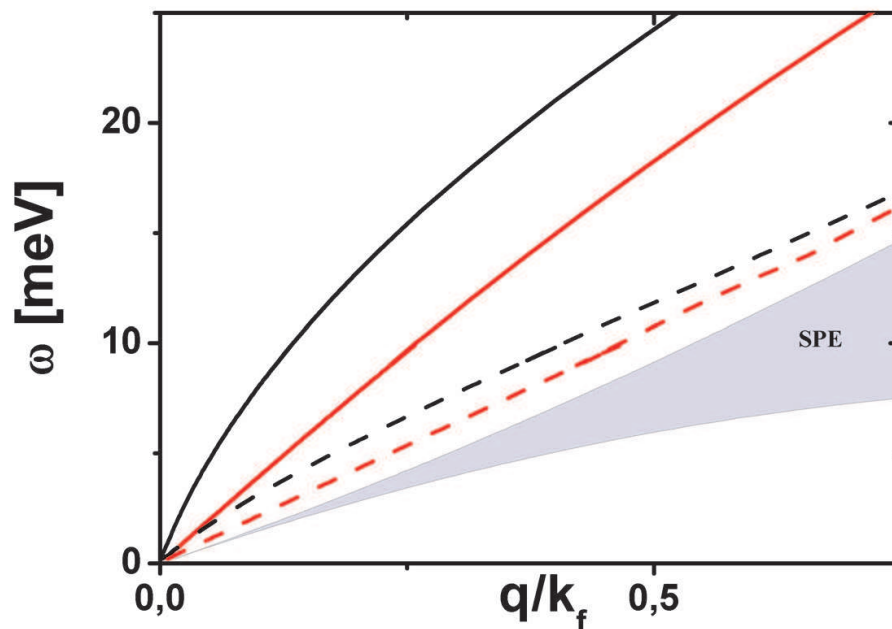
Fig. 9. The optical ω_+ (black branches) and acoustical ω_- (red branches) plasmons for the background values: (i) $\epsilon_0 = 1$ (solid-line branches) and (ii) $\epsilon_0 = 3.9$ (dashed-line branches). The Fermi wavevector $k_f = 0.7x10^6 \ cm^{-1}$ and the sample parameters are $L_1 = L_2 = 20$ nm. We keep $\beta = 0$.

is written in terms of both the noninteracting polarizability function,

$$\Pi_{mn}(k,q,\omega) = g_v g_s \frac{f\left[E_m(k)\right] - f\left[E_n(k+q)\right]}{E_m(k) - E_n(k+q) - \hbar\omega - i\delta\hbar}, \tag{16}$$

with g_v and g_s being the valley and spin degeneracy, respectively, and the total Coulomb potential $V \equiv V^{ext} + V^s$, where V^{ext} is the external potential. The wavevector q is the usual transferred momentum due to Coulomb interaction and ω is the external frequency. Since the total potential $V_{mn}(k,q)$ in Eq. (15) is a function of two wave-vectors, one should Fourier transform the potential $V^s(r)$, and take advantage from Eq. (15), to write

$$V^s_{mn}(k,q,\omega) = \frac{1}{L_y} \sum_{m',n',k',q'} \Pi_{m'n'}(k',q',\omega) \times$$

$$v_{mnm'n'}(k\prime,k,q) \times V_{m'n'}(k\prime,q'), \tag{17}$$

where

$$v_{mnm'n'}(k,k',q) = \frac{2e^2}{\epsilon_0} \int dx' \int dx \ \phi^*_{m,k}(x)\phi_{n,k+q}(x) \times$$

$$K_0(q\,|x - x'|)\phi^*_{m',k'+q}(x')\phi_{n',k'}(x'). \tag{18}$$

Here, K_0 is the zero-order modified Bessel function of the second kind.

The 1D spatial confinement used here couples the motion in the x-direction to the motion in the y-direction through the wavevector k, leading $v_{mnm'n'}$ to be dependent also on the wavevectors k and k'. We mention that this turns out to be a difficulty, since it

makes the dielectric function depends not only on the wave-vector q, but also on the wavevectors k and k'(Brey & Fertig, 2007). As a matter of fact, for 1D semiconductor systems (Wendler & Grigoryan, 1996; Xia & Hai, 2002) in the presence of perpendicular magnetic field, this difficulty has been overcame by treating the k and the spatial dependencies separated from each other, and expanding the wavefunction in a perturbation series in such a way that the dielectric function could be projected into a finite submatrix, whose dimension is the same as the perturbation order. In this work, we also overcome this difficulty by using the same technique and further taking the advantage from the natural relation between the pseudo-spinors components.

Notice first that the spinor component

$$\phi_{nk}^{B}(x) = -\frac{i\gamma}{[E_n(k) + \beta]}\left[\frac{d\phi_{nk}^{A}}{dx} - k\phi_{nk}^{A}\right] \tag{19}$$

can be written in terms of its counterpart $\phi_{nk}^{A}(x)$ by virtue of the symmetry of the Eq. 1 only. This leads the Coulomb potential form factor to be written as

$$v_{mnm'n'}(k, k', q) = -\gamma^2\eta A_{mnm'n'}^{(0)} + A_{mnm'n'}^{(1)}k' + A_{mnm'n'}^{(2)}k'^2 + A_{mnm'n'}^{(3)}, \tag{20}$$

where

$$\eta(k', q) = [(E_m(k') + \beta)(E(k' + q) + \beta)]^{-1},$$

and

$$A_{mnm'n'}^{\mu} = a_{mnm'n'}^{(0,\mu)} + a_{mnm'n'}^{(1,\mu)}k + a_{mnm'n'}^{(2,\mu)}k^2 \text{ with } (\mu = 0, 1, 2, \text{ and } 3).$$

Secondly, notice that the k'-dependence in Eq. (20) has been explicitly taken out. The coefficients $a_{ijmn}^{(0,\mu)}(k, q)$, $a_{ijmn}^{(1,\mu)}(k, q)$, and $a_{ijmn}^{(2,\mu)}(k, q)$ for $\mu = 0, 1, 2$, and 3 are shown in the Appendix B and involves the spatial integrals shown in Eq. (18). The summation of the terms on k' appearing in the Eq. (20) does not arise as a consequence of any perturbative approach on $\psi_{nk}(x, y)$.It rather shows up directly due to the nature of the Dirac equation, leading to the Eq. (19). At this point, and in order to get the exact dielectric constant as a function of q and ω only, we use the same technique as in Refs. (Li & Das Sarma, 1991; Rodríguez & Tejedor, 1994) and define

$$X_{mn}(q, \omega) = \frac{1}{L_y}\sum_{k}V_{mn}^{s}(k, q, \omega), \tag{21}$$

so that the dynamically dielectric function come out straightforwardly after the standard procedure in obtaining the relation $\varepsilon(q, \omega) = V^s/V$.

Because of the weak tunneling condition and provided the system we are considering in this paper is symmetric ($L_1 = L_2$ in Fig. 1), there are only two different elements of v, i.e., $v_{1111}(q, k, k') = v_{2222}(q, k, k') = V_A$ and $v_{1122}(q, k, k') = v_{2211}(q, k, k') = V_C$. (Tavares & Hai, 2000) Furthermore, in this work we consider the same 1D charge density $N_{1D} = 2k_F/\pi$ (with $k_F = 0.7 \times 10^6 cm^{-1}$) for both waveguides, so that the polarizability $\Pi_{11} = \Pi_{22} = \Pi_0(k, q, \omega)$. The collective excitation spectra is then obtained through the condition of vanishing determinant of the matrix $\varepsilon(q, \omega)$. This condition leads to the equation $\varepsilon_+\varepsilon_- = 0$, where

$$\varepsilon_{\pm}(q,\omega) = \left[1 - \sum_{k,k'}(V_A \pm V_C)\Pi_0\right].\tag{22}$$

The roots of $\varepsilon_+ = 0$ and $\varepsilon_- = 0$ provide the in-phase optical and out-phase acoustic plasmon modes, respectively. These modes can be observed via inelastic light scattering spectroscopy experiments. The acoustic mode represents densities in the two wires fluctuating out of phase, whereas the optical mode represents densities in two wires fluctuating in phase. In the following, we analyze these modes carefully.
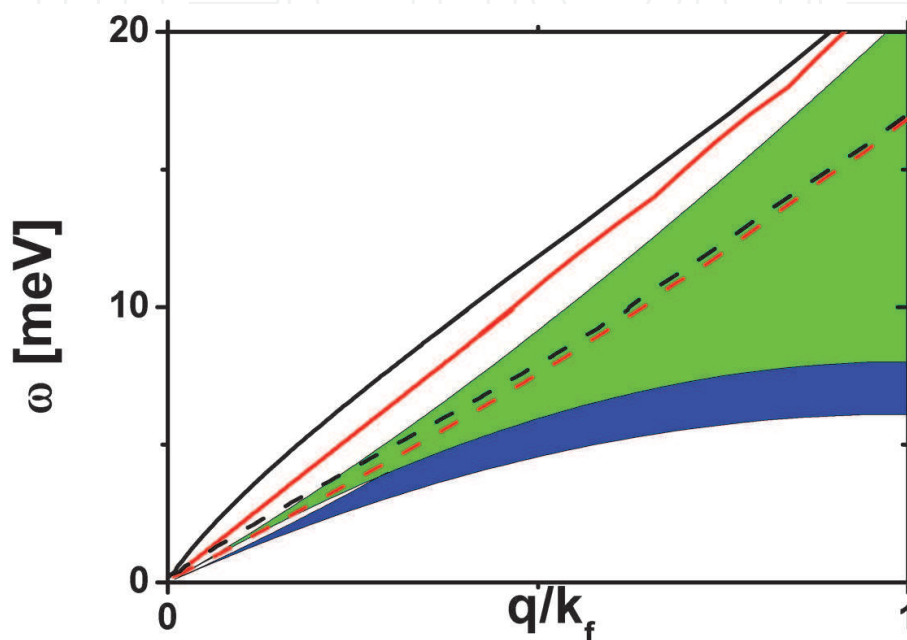
Fig. 10. The optical ω_+ (black branches) and acoustical ω_- (red branches) plasmons for different values of the parameter β : (i) $\beta = 0$ (solid-line branches) and (ii) $\beta = 75 meV$ (dashed-line branches). The Fermi wavevector and the sample parameters are the same as in the previous Figure. Here we keep $\epsilon_0 = 3.9$. The green [blue] continuum is the SPE region for the case (i) [(ii)].

4.3 Results and discussions

Firstly, let us discuss the interesting effects that different choices for the *background* dielectric constant ϵ_0 have on the response functions ε_+ and ε_- and, as consequence, on the plasmon dispersion relation. This dielectric constant accounts for the kind of material that serves as a substrate over which the graphene sheet is eventually deposited. Here, we take two values for it: (i) $\epsilon_0 = 1$ and (ii) $\epsilon_0 = 3,9$. The first one represents the most elementar case where the graphene sheet is suspended, while the case (ii) represents SiO_2 as a substrate over which the graphene sheet is deposited. The goal here is to show the effects of continuously changing ϵ_0 on the plasmon modes and also on the single-particle excitations (SPE). For such a purpose, we show in Fig.9 the dispersion relation of the acoustic $\omega_-(q)$ (red branches) and optical $\omega_+(q)$ (black branches) plasmon modes, as a function of the transferred wavevector q, for the two values of ϵ_0 discussed above. The solid lines represent the results for $\epsilon_0 = 1$, while results for $\epsilon_0 = 3,9$ are shown in dashed lines. The shadow area is the continua where SPE occurs.

These excitations are defined by a continuum region in the ω-q space where $Im[\Pi_0(q,\omega)] \neq 0$ and are responsible for Landau damping the plasmon modes as they enter into (or approach to) the shaded continuum. As ϵ_0 increases, the plasmons get closer and closer to the SPE continuum. These results then suggest that these modes should be experimentally seen more easily for materials with less values of ϵ_0, since they are far from the Landau damping region. At this point we should briefly mention that, in the presence of effective tunneling between the wells, the acoustic mode $\omega_-(q)$ in Fig.9 should present a non-zero value in the long wavelength limit $q \rightarrow 0$. The same behavior certainly occurs if $\epsilon_0 = 11,68$, which corresponds to the background value for GaAs. Despite of it, the results presented here should not be much different when an effective, but still weak, tunneling is considered. Moreover, these results turn out be the first step in theoretically approaching tunneling effects, which is certainly responsible for losing guidance efficiency in the ballistical waveguides. In Fig. 10, we choose to show the same results as in Fig. 9, but now varying the parameter β and keep the dielectric constant $\epsilon_0 = 3.9$. As the parameter β increases, the SPE continuum changes accordingly. Such an effect on the SPE mimics an re-scaling of the Fermi surface as the parameter β increases.

5. Conclusion

In summary, we have studied single-particle properties of Dirac Fermions laterally confined to coupled double wire graphene structures which are being embedded over different substrates, and explored for 2D and 1D transport recently. We have added an ad-hoc term to the pseudo-relativistic Dirac equation which controls the interaction between graphene sheets and the substrate. Both the strength of this interaction as well as the spatial asymmetry on the double wire structures can affect the extended and localized character of states and the shape of the minima in the energy dispersion of the lowest subbands. We may claim that these effects will manifest themselves on the quantum conductance of the system and, eventually, changing the conductance plateau from $16e^2/h$ to $8e^2/h$. We also have shown the existence of guided modes up to the seventh order in single and double waveguides based on graphene. Our results also show that different choices for β in both waveguides induces spatial anisotropy effects on the guided modes, reflecting anomalous effects on their probability density functions. We believe that these results are timely and may stimulate further theoretical and experimental investigations on these graphene based structures.

We also have theoretically studied the acoustical and optical plasmon modes in coupled graphene quantum wires in the extremely weak tunneling regime. In particular, attention was devoted to the effects induced by the interaction between the graphene sheet and the substrate. This interaction has been considered through an *ad-hoc* parameter β in the 2D Dirac-like Hamiltonian modeling a more general diatomic system in which the graphene lattice sites A and B might have different number of electrons. We have calculated the Coulomb potential elements for this massless Fermion gas. We have shown that the parameter β might be serving to screen the Coulomb interaction in the system. Such an effect manifests itself in the dispersion relation of the optical and acoustical plasmon modes. We found that the parameter β should eventually increase the damping effects on these modes.

6. Acknowledgments

7. Appendix A

The 8×8 matrix $\hat{M}$ is given by

$$
\begin{bmatrix}
\frac{f_-(E+\beta_{II})L}{\gamma e^{-\kappa_I\theta}} & m_{12} & m_{13} & 0 & 0 & 0 & 0 & 0 \\
0 & m_{22} & m_{23} & m_{24} & m_{25} & 0 & 0 & 0 \\
0 & 0 & 0 & m_{34} & m_{35} & m_{36} & m_{37} & 0 \\
0 & 0 & 0 & 0 & 0 & m_{46} & m_{47} & \frac{f_+(E+\beta_{IV})L}{\gamma e^{-\kappa_I\delta}} \\
e^{-\kappa_I\theta} & \sin q_{II}\theta & -\cos q_{II}\theta & 0 & 0 & 0 & 0 & 0 \\
0 & \sin q_{II}\sigma & -\cos q_{II}\sigma & e^{-\kappa_{III}\sigma} & e^{\kappa_{III}\sigma} & 0 & 0 & 0 \\
0 & 0 & 0 & e^{\kappa_{III}\sigma} & e^{-\kappa_{III}\sigma} & -\sin q_{IV}\sigma & -\cos q_{IV}\sigma & 0 \\
0 & 0 & 0 & 0 & 0 & -\sin q_{IV}\delta & -\cos q_{IV}\delta & e^{-\kappa_I\delta}
\end{bmatrix}, \quad (23)
$$

where

$$
\begin{aligned}
m_{12} &= L(k_y \sin q_{II}\theta + q_{II}\cos q_{II}\theta), & m_{13} &= L(q_{II}\sin q_{II}\theta - k_y\cos q_{II}\theta), \\
m_{22} &= L(k_y \sin q_{II}\sigma + q_{II}\cos q_{II}\sigma), & m_{23} &= L(q_{II}\sin q_{II}\sigma - k_y\cos q_{II}\sigma), \\
m_{24} &= L\gamma^{-1}g_-(E+\beta_{II})e^{-\kappa_{III}\sigma}, & m_{25} &= L\gamma^{-1}g_+(E+\beta_{II})e^{\kappa_{III}\sigma}, \\
m_{34} &= L\gamma^{-1}g_-(E+\beta_{IV})e^{-\kappa_{III}\sigma}, & m_{35} &= L\gamma^{-1}g_+(E+\beta_{IV})e^{\kappa_{III}\sigma}, \\
m_{36} &= L(q_{IV}\cos q_{IV}\sigma - k_y\sin q_{IV}\sigma), & m_{36} &= -L(k_y\cos q_{IV}\sigma + q_{IV}\sin q_{IV}\sigma), \\
m_{46} &= L(q_{IV}\cos q_{IV}\delta - k_y\sin q_{IV}\delta), & m_{36} &= -L(k_y\cos q_{IV}\delta + q_{IV}\sin q_{IV}\delta).
\end{aligned}
$$

Here, we also define $f_\pm = \gamma(k_y \pm \kappa_I) / (E - U + \beta_I)$, $g_\pm = \gamma(k_y \pm \kappa_{III}) / (E - U + \beta_{III})$, $\theta = (2L_1 + L_b)/2$, $\sigma = L_b/2$, and $\delta = (2L_2 + L_b)/2$.

8. Appendix B

The coefficients $a_{ijmn}^{(0,\mu)}(k,q)$, $a_{ijmn}^{(1,\mu)}(k,q)$ and $a_{ijmn}^{(2,\mu)}(k,q)$ for $\mu = 0,...,3$ are related to the expansion of the Coulomb form factor and have the following form:

$$
\begin{aligned}
a_{ijmn}^{(0,0)}(k,q) = \frac{2e^2}{\epsilon_0} \int dx' \int dx [\phi_{A,i}(x)\phi_{A,j}(x) + \gamma^2\eta(\phi_{A,i}'(x)\phi_{A,j}'(x) + \\
q\phi_{A,i}'(x)\phi_{A,j}(x))]K_0(q\,|x-x'|)[\phi_{A,m}'(x')\phi_{A,n}'(x') + q\phi_{A,m}'(x')\phi_{A,n}(x')].
\end{aligned}
$$

9. References

Ando, T.; & Nakanishi, T. (1998). Impurity Scattering in Carbon Nanotubes - Absence of Back Scattering. *J. Phys. Soc. Jpn.* Vol. 67, (1998) 1704-1713.

Ando, T.; (2006). Screening Effect and Impurity Scattering in Monolayer Graphene. *J. Phys. Soc. Jpn.* Vol. 75, (2006) 074716.

Beenakker, C. W. J. (2008). Colloquium: Andreev reflection and Klein tunneling in graphene. *Rev. Mod. Phys.* Vol. 80, (2008) 1337–1354

Beenakker, C.W. J.; Sepkhanov, R. A.; Akhmerov, A. R.; & Tworzydło, J. (2009). Quantum Goos-Hanchen effect in graphene. *Phys. Rev. Lett.* Vol. 102, (2009) 146804-146808

Berry, M. V.; & Mondragon, R. J. (1987). Neutrino billiards: time-reversal symmetry-breaking without magnetics fields. *Proc. R. Soc. Lond. A.* Vol. 412, (1987) 53-74

Bostwick, A.; Ohta, T.; Seyller, T.; Horn, K.; & Rotenberg, E. (2007). Quasiparticle dynamics in graphene. *Nature Physics.* Vol. 3, (2007) 36 - 40

Brey, L.; Fertig, H. A. (2006). Electronic states of graphene nanoribbons studied with the Dirac equation. *Phys. Rev. B,* Vol. 73, (2006) 235411-235416

Brey, L.; & Fertig, H. A.; (2007). Elementary electronic excitations in graphene nanoribbons. *Phys. Rev. B* Vol. 75, (2007) 125434-125440

Castro Neto, A. H.; Guinea, F.; Peres, N. M. R.; Novoselov, K. S.; & Geim, A. K. (2009). The electronic properties of graphene. *Rev. Mod. Phys,* Vol. 81, (2009) 109–162

Castro Neto, A. H. (2010). The carbon new age. *Materialstoday,* Vol. 13, (2010) 12-17

Cheianov, V. V.; Fal'ko, V.; & Altshuler, B. L. (2007). The Focusing of Electron Flow and a Veselago Lens in Graphene p-n Junctions. *Science,* Vol. 315, (2007) 1252-1255

Chiu, H-Y.; Perebeinos, V.; Lin, Y-M.; & Avouris, P. (2010). Controllable p-n Junction Formation in Monolayer Graphene Using Electrostatic Substrate Engineering. *Nano Letters*, Vol. 10, (2010), 4634–4639

Hwang, E. H.; & Das sarma, S. (2007). Dielectric function, screening, and plasmons in two-dimensional graphene. *Phys. Rev. B,* Vol. 75, (2007) 205418-205424

Das Sarma, S.; Adam, S.; Hwang, E. H.; Rossi, E. (2010). Electronic transport in two dimensional graphene. *arXiv:1003.4731v2*

Ehrenreich, H.; & Cohen, M. H. (1959). Self-Consistent Field Approach to the Many-Electron Problem. *Phys. Rev.* Vol. 115, (1959) 786-790

Giovannetti, G.; Khomyakov, P. A.; Brocks, B.; Kelly, P. J.; & van den Brink, J. (2007). Substrate-induced band gap in graphene on hexagonal boron nitride: Ab initio density functional calculations. *Phys. Rev. B,* Vol. 76, (2007) 073103-073107

Goos, F.; & Hanchen, H. (1947). Ein neuer und fundamentaler versuch zur totalreflexion. *Ann. Phys.* Vol. 1, (1947) 333-346

Jackson, J. D. (1998). Classical Electrodynamics. *New York: John Wiley & Sons*, (1998).

Kane, C. L.; & Mele, E. J. (2005). Quantum spin Hall effect in graphene. *Phys. Rev. Lett*, Vol. 95, (2005) 226801-226805

Katsnelson, M. I.; Novoselov, K. S.; & Geim, A. K. (2006). Chiral tunnelling and the Klein paradox in graphene. *Nature Phys.* Vol. 2, (2006) 620-625

Li, Q. P.; & Das Sarma, S. (1991). Elementary excitation spectrum of one-dimensional electron systems in confined semiconductor structures: Finite magnetic field. *Phys. Rev. B*, Vol. 44, (1991) 6277–6283

Lin, Y.-M.; Perebeinos, V.; Chen, Z.; & Avouris P. (2008). Electrical observation of subband formation in graphene nanoribbons. *Phys. Rev. B* Vol. 78, (2008) 161409-161413

Lu, Y. H.; He, P. M.; & Feng, Y. P. (2007). Graphene on metal surface: gap opening and n-doping. *arXiv:0712.4008v1*

Min, H.; Hill, J. E.; Sinitsyn, N. A.; Sahu, B. R.; Kleinman, L.; & MacDonald, A. H. (2006). Intrinsic and Rashba spin-orbit interactions in graphene sheets. *Phys. Rev. B,* Vol. 74, (2006) 165310-165315

Miao, F.; Wijeratne, S.; Zhang, Y.; Coskun, U. C.; Bao, W.; & Lau, C. N. (2007). Phase-coherent transport in graphene quantum billiards. *Science,* Vol. 317, (2007) 1530-1533

Nguyen, H.C.; Hoang, M.T.; & Nguyen, V.L. (2009). Quasi-bound states induced by one-dimensional potentials in graphene. *Phys. Rev. B.* Vol. 79 (2009) 035411-035417

Novoselov, K. S.; Geim, A. K.; Morozov, S. V. ; Jiang, D.; Zhang, Y.; Dubonos, S. V.; Grigorieva, I. V.; & Firsov, A. A. (2004). Electric field effect in atomically thin carbon films. *Science,* Vol. 306, (2004) 666-669.

Pereira, J. M.; Mlinar, V.; Peeters, F. M.; & Vasilopoulos, P. (2007). Confined states and direction-dependent transmission in graphene quantum wells. *Phys. Rev. B,* Vol. 74 (2007) 045424-045428

Pereira, J. M.; Mlinar, V.; Peeters, F. M.; & Vasilopoulos, P. (2007). Confined states and direction-dependent transmission in graphene quantum wells. *Phys. Rev. B,* Vol. 74 (2007) 045424-045428

Peres, N. M. R.; Rodrigues, J.N.B.; Stauber, T.; & Lopes dos Santos, J. M. B. (2009). Dirac electrons in graphene-based quantum wires and quantum dots. *J. Phys.: Condens. Matter,* Vol. 21, (2009) 344202-344220

Peres N. M. R. (2010). Colloquium: The transport properties of graphene: An introduction. *Rev. Mod. Phys,* Vol. 82, (2010) 2673-2700

Ritter, K. A.; & Lyding, J. W. (2009). The influence of edge structure on the electronic properties of graphene quantum dots and nanoribbons. *Nature Materials* Vol. 8, (2009) 235 - 242

Rodríguez, F. J.; & Tejedor, C. (1994). Nonlocal interaction and Fermi-edge singularities in quasi-one-dimensional systems with a transverse magnetic field. *Phys. Rev. B* Vol. 49, (1994) 16781-16784

Semenoff, Gordon W. (1984). Condensed-Matter simulation of a three-dimensional anomaly. *Phys. Rev. Lett.* Vol. 53, (1984) 2449–2452.

Son, Y-W; Cohen, M. L.; & Louie, S. G. (2006). Energy gaps in graphene nanoribbons. *Phys. Rev. Lett.* Vol. 97, (2006) 216803-216807

Tavares, M.R.S. & Hai, G.-Q. (2000). Inelastic Coulomb scattering rates due to acoustic and optical plasmon modes in coupled quantum wires. *Phys. Rev. B* Vol. 61, (2000) 7564-7570

Villegas, C. E. P.; & Tavares, M. R. S. (2010). Strongly coupled modes in bi-waveguides based on graphene. *Solid state communications,* Vol 150 (2010) 1350-1354

Villegas, C. E. P.; Tavares, M. R. S.; & Marques, G. E. (2010). Anisotropy induced localization of pseudo-relativistic spin states in graphene double quantum wire structures. *Nanotechnology*, Vol 21, (2010) 365401-365407

Villegas, C. E. P.; & Tavares, M. R. S. (2010). Substrate interaction effects on optical and acoustical plasmons in bi-waveguides based on graphene. *Diamond and related Materials*, Vol 20, (2011) 170-173

Wendler, L.; & Grigoryan, V. G. (1996). Collective and single-particle excitations of the quasi-one-dimensional electron gas in the presence of a magnetic field. *Phys. Rev. B,* Vol. 54, (1996) 8652-8675

Williams, J. R.; DiCarlo, L.; & Marcus, C. M. (2007) Quantum Hall effect in a gate-controlled p-n junction of graphene. *Science,* Vol. 317, (2007) 638-641.

Williams, J. R.; Low, T.; Lundstrom, M. S.; & Marcus, C. M. (2011) Gate-controlled guiding of electrons in graphene. *Nature Nanotechnology,* Vol. 6, (2011) 222–225

Xia, J.-B.; & Hai, G.-Q. (2002). Collective and single-particle excitations in coupled quantum wires in magnetic fields. *Phys. Rev. B* Vol. 65, (2002) 245326-245331

Yakes, M.K. *et al.* (2010). Conductance Anisotropy in Epitaxial Graphene Sheets Generated by Substrate Interactions. NanoLetters Vol 10**,** (2010) 1559-1562

Zhang, L. M.; & Fogler, M. M. (2008). Nonlinear Screening and Ballistic Transport in a Graphene p-n Junction. *Phys. Rev. Lett.* Vol. 100, (2008) 116804-116808.

Zhou, S. Y.; Gweon, G.-H.; Fedorov, A. V.; First, P. N.; De Heer, W. A.; Lee, D.-H.; Guinea, F.; Castro Neto, A. H.; & Lanzara, A. (2007). Substrate-induced bandgap opening in epitaxial graphene. *Nature Mater.* Vol. 6, (2007) 770-775.

Ziegler, K. (1996). Dirac fermions with disorder in two dimensions: Exact results. *Phys Rev. B.* Vol. 53, (1996) 9653-9657.
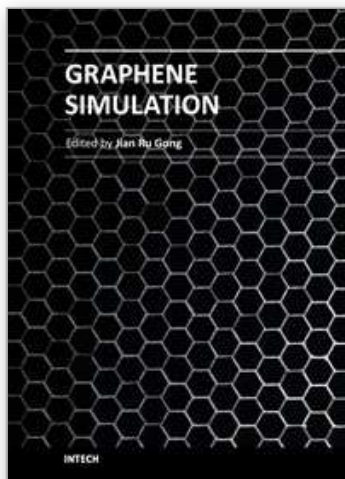
Graphene Simulation

Edited by Prof. Jian Gong

Graphene, a conceptually new class of materials in condensed-matter physics, has been the interest of many theoretical studies due to the extraordinary thermal, mechanical and electrical properties for a long time. This book is a collection of the recent theoretical work on graphene from many experts, and will help readers to have a thorough and deep understanding in this fast developing field.

How to reference

In order to correctly reference this scholarly work, feel free to copy and paste the following:

INTECH
open science | open minds